

Z. F. Wang · W. Cao · Z. Lu

MOEMS: packaging and testing

Received: 24 June 2004 / Accepted: 14 February 2005 / Published online: 11 October 2005
© Springer-Verlag 2005

Abstract In this paper, packaging techniques of fiber optical MEMS devices are investigated. A packaging scheme is proposed, which includes the architecture to construct the component package and the major packaging flow to implement it. Passive fiber alignment with the accuracy comparable with active alignment is presented by the combination of rectangular shape fiber grooves and micro fiber stoppers. The experimental setup specific for fiber optic MEMS component is presented for the fiber assembly and the characterization of optical loss. A testing system based on the Labview 6.1 instrument control is also presented, which can facilitate the characterization of switching time for MEMS optical switches.

1 Introduction

The growth of fiber optic networks is driving the development of small, low cost and high performance optical components based on microelectromechanical system (MEMS) technology. Packaging has turned to be a bottleneck technology in commercializing the recently developed fiber optic MEMS devices or subsystems, which have revealed promising performance in wafer level implementation. The purpose of packaging a fiber optic MEMS device is to house the chip, protect the structures from mechanical shock and humidity transmission, establish the optical paths by pigtailling the chip with optical fibers, and provide electrical connection for

control. The requirement of low insertion loss would ask for the appropriate selection of an optical fiber with certain specifications. Precision fiber assembly with high alignment accuracy is paramount as well for achieving a low coupling loss. Furthermore, the precision and repeatability of fiber bonding process also affects the optical loss of the packaged component.

In this paper, packaging techniques of fiber optical MEMS devices are investigated. A packaging scheme is proposed, which includes the architecture to construct the component package and the major packaging flow to implement it. The experimental setup specific for fiber optic MEMS components is presented for the fiber assembly and the characterization of optical loss. A testing system based on the Labview 6.1 instrument control is also presented, which can facilitate the characterization of switching time for MEMS optical switches.

2 Packaging

A two-level packaging scheme was applied in the prototyping. Fig. 1 illustrates the schematics of this package structure. A core package, named as subpackage, was built up as the first level package of the MEMS device. It consisted of three parts: substrate, frame and glass lid. The ceramic substrate with the MEMS chip seating on after wirebonding, was bonded with a ceramic frame to enfold the chip. The ceramic frame was fabricated through laser scribing and cutting. Slots were formed on the ceramic frame for fitting the optical fibers. A glass lid was then bonded using epoxy. All the electrical connection and fiber assembly with the chip were implemented within the subpackage, which was then encapsulated in a metal case as the final package. The packaging work was completed by pigtailling the metal case with optical fibers and a plug-in electrical connector, followed by sealing the case with a cover.

Figure 2 illustrates the experimental setting for fiber assembly work and some optical tests. The positioning

Z. F. Wang (✉) · W. Cao
Singapore Institute of Manufacturing Technology,
71 Nanyang Drive, 638075 Singapore, Singapore
E-mail: zfwang@SIMTech.a-star.edu.sg
Tel.: +65-6793-8596
Fax: +65-6792-2779

Z. Lu
National University of Singapore, Singapore, Singapore

Fig. 1 Schematics of optical MEMS package

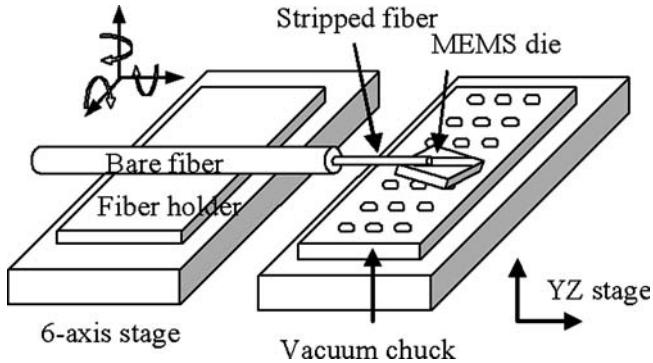
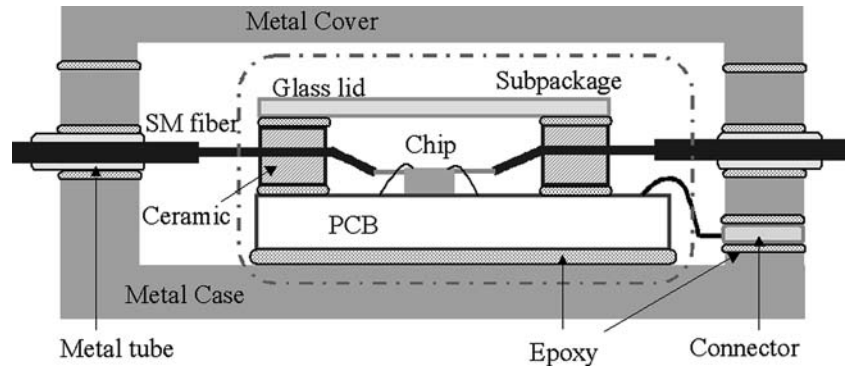


Fig. 2 Workstation for fiber assembly

stage could be operated either manually or semi-automatically through the electrostrictive actuators, which can be applied for fiber coupling tests in free space when aided by a detector and an alignment controller.

An adhesive bonding system was integrated on the optical workstation to facilitate epoxy dispensing and curing on the miniaturized objective. A liquid barrel with dispensing tip was assembled on a positioning stage, which enhanced the positioning precision of dispensing spot up to 1 μm under manual adjustment or 20 nm under automatic tuning aided by the electrostrictive actuators. An automatic dispenser was equipped to provide small dispensing volume of epoxy. A spot UV-curing system was installed on the workstation and connected with the dispenser. A two-way light guide (3 mm in diameter) was placed symmetrically above the workbench for eliminating the shadow effect during adhesive curing. By customizing the fixture, the two tips of light guide were adjustable in direction towards and away from the objective under curing.

In the optical MEMS devices being packaged, optical paths are constrained by rectangular shape grooves, called U-grooves, and fiber stoppers, as shown in Fig. 3. The grooves and fiber stoppers were patterned and formed simultaneously with the MEMS structures, e.g. mirror, actuator and spring, during the MEMS fabrication. The optical fiber, with the same diameter as the groove width, was clamped into a vertical reference plane by fiber stoppers, and subsequently the fiber stoppers were slightly bent once the fiber was embedded.

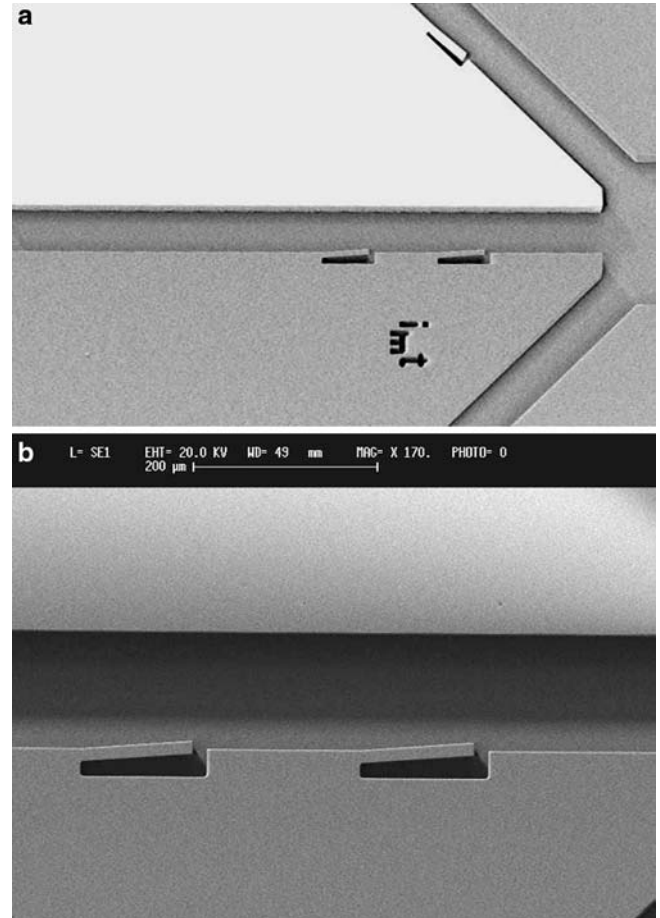


Fig. 3 Fiber groove and fiber stopper (SEM)

Consequently the spring force prevented the fiber from out-of-plane displacement and limited the alignment error to within the eccentricity of the fiber cores and the variation of the fiber diameter.

In our experiment, U-grooves, instead of V-grooves as commonly adopted, were effectively facilitating the fiber alignment work and revealed promising performance. No significant misalignment was observed during the fiber assembly process because of the specific design of grooves and stoppers. This was well proven by a comparison test, as depicted in Fig. 4. The comparison

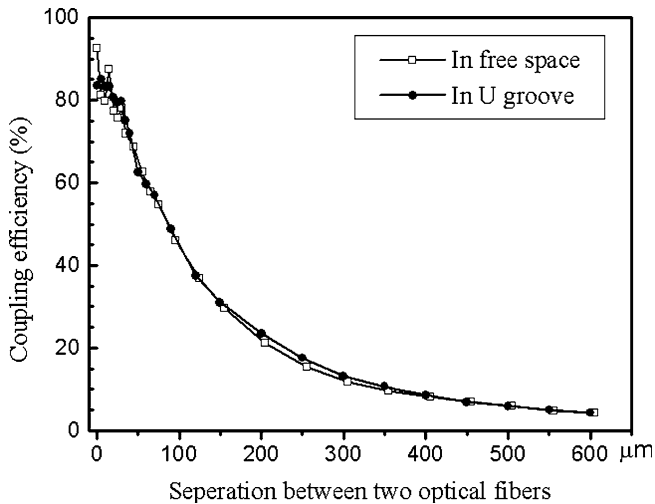


Fig. 4 Comparison test for fiber coupling

test was set to evaluate the coupling loss introduced by the fiber assembly. This coupling loss measurement was applied towards two normal cleaved single mode fibers and targeting the relation between coupling efficiency and fiber-to-fiber distance. One curve in Fig. 4 is the result of active alignment under an automatic fiber alignment system, which stands for the maximum coupling efficiency in free space. Another curve is the result of measurement under passive alignment, when the two fibers were embedded in fiber grooves. The good coincidence between these two curves indicates a satisfactory accuracy for the presented fiber assembly method.

Three adhesives, NEA121, NOA61 and NOA81 were evaluated in the fiber-to-chip bonding process under the identical set of working parameters. UV curing was done immediately after the epoxy dispensing without moving the bonding objective. The joining quality of the fiber-to-chip bonding was characterized under retention test. Before the test, the cross section was inspected under a microscope. It was assured that the epoxy had filled the gap between fiber and groove and covered the exposed part of fiber. Moreover, the cross section view shows that the fiber was deposited in the groove precisely without any significant gap that would cause misalignment. The similar cross section images were observed on a number of samples. Such precise and repeatable fiber positioning is believed to be responsible for the test result shown in Fig. 4. The fiber assembly process developed in this experiment could ensure the positioning accuracy between fiber and groove and therefore, reduce the coupling loss due to misalignment of fibers.

The epoxy bonding strength at the fiber-to-chip joint was evaluated by tensile test. MEMS chip, which was bonded with a bare single mode fiber in groove, was mounted on a ceramic plate for test. The test fixture was customized to hold bare fiber, which was typically 250 μm in diameter and extremely fragile. Samples bonded with different epoxies were tested under identical conditions. Throughout the retention test, no debonding

had been observed at the fiber-to-chip joint. Such results indicate the good bonding quality in the joining part. Fig. 5 shows the experimental setting.

After wirebonding and fiber assembly, the subpackage was subsequently sealed by filling the fiber slot with NEA123A and covering the glass lid with Loctite 3311, which was then put into a customized bombing chamber for helium test. The result indicated that the leakage rate of the hermetically sealed subpackage was lower than 10^{-7} std cc/s (Jin et al. 2002).

The fiber retention tests were then conducted towards the fiber pigtailing on Instron. A metal case was fixed on the workbench after connecting with optical fiber. Fiber with loose rubber tube was clamped above the sample by a test fixture. The pulling force was continuously increased till debonding happened. Each straight pull lasted 5 s and was repeated three times. The results indicate that by using NEA123S, the fiber interconnection could withstand loading weight more than 1.0 kg, which is required by the corresponding Telecordia document (generic requirements for singlemode fibre optic switches 2001). It was noted that throughout the retention test, no failure had been observed on the joints between metal tube and the case. Figure 6 illustrates a packaged MEMS optical switch, exclusive of the cover.

3 Testing

As the essential parameters of the optical switch, insertion loss, return loss, and switch time were characterized by using a 1×4 MEMS optical switch (Wang et al. 2002) as test vehicle following the procedures and requirements of international standards (generic requirements

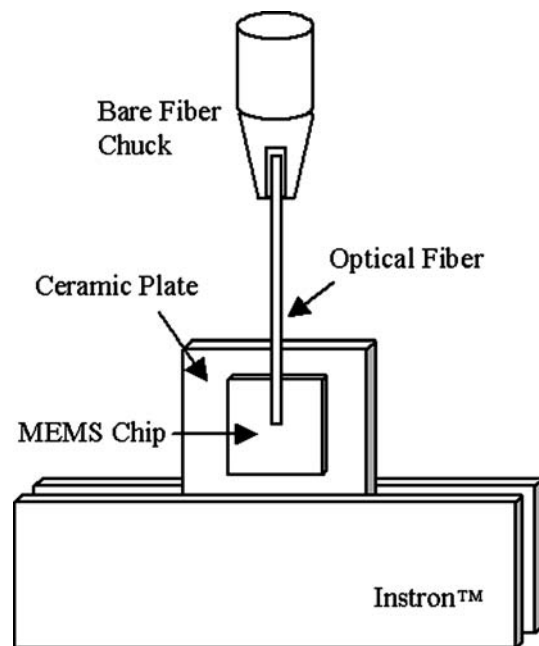
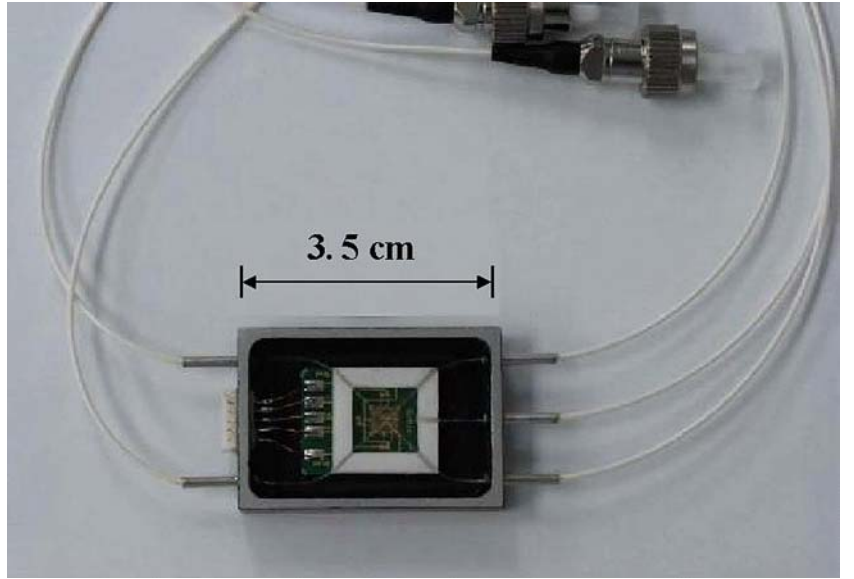


Fig. 5 Diagram of fiber-chip tensile test

Fig. 6 Packaged optical MEMS



for singlemode fibre optic switches 2001; TIA/EIA standard 1995, 1999). The test equipment included DFB source module and power detector module in Newport 8800, detector module in ORINON fiber auto-alignment system, Newport F-CPL-S12155 coupler (1×2 type), and the fiber adaptors. The center operating wavelength is 1,550 nm.

The insertion loss is the fraction of power transferred from input port i to output port j expressed in units of dB [2]. Insertion loss depends on the input–output connection (i, j), wavelength, and also on the switch state. The insertion loss of connection (i, j) at wavelength λ and a given switch state is designated $IL_{ij}(\lambda)$ and is defined by the following equation:

$$IL_{ij}(\lambda) = -10\text{Log}_{10} \frac{P_j(\lambda)}{P_i(\lambda)}, \quad (1)$$

where, $P_i(\lambda)$ is the optical power launched into port i at center wavelength λ and $P_j(\lambda)$ is the on-state optical power measured at port j at center wavelength λ and a given switch state. The measurement scheme of insertion loss is illustrated in Fig. 7. The power launched in the optical switch, P_i , was calculated using the readings of power output of port3, P_{ref} . The insertion loss is expressed as:

$$IL = -10\text{Log}_{10} \frac{P_j}{kP_{\text{ref}}}, \quad (2)$$

where, k is the coupling ratio.

The insertion losses in two states, bar state and cross state, were characterized. All the readings were taken repeatedly in order to reflect the errors caused by the connect difference. The characterization results and their distributions depicted in Fig. 8 exhibit considerable repeatability.

Return loss measures the cumulative effect of all backscatter and parasitic reflections from within the device. Return loss depends on the port, wavelength, and may depend on the switch state (generic requirements for singlemode fibre optic switches 2001).

$$RL_i(\lambda) = -10\text{Log}_{10} \frac{P_{i(\text{back})}(\lambda)}{P_{i(\text{in})}(\lambda)}, \quad (3)$$

where $P_{i(\text{in})}(\lambda)$ is the optical power launched into port i , and $P_{i(\text{back})}(\lambda)$ is the off-state optical power returning to port i at center wavelength λ .

Following the measurement procedure in TIA/EIA Standard (1999), the characterization scheme was set up as Fig. 9a and b. The power levels P_0 at the detector at coupler port 1 and P_1 at the detector at coupler port 3

Fig. 7 Measurement setup of insertion loss

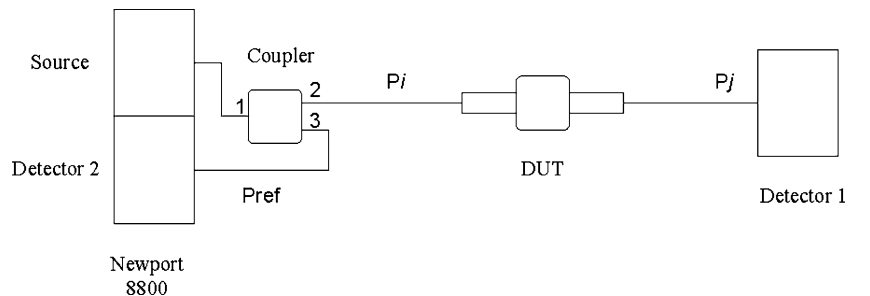


Fig. 8 Insertion losses and their distributions (a) Insertion loss: bar state (b) Insertion loss: cross state

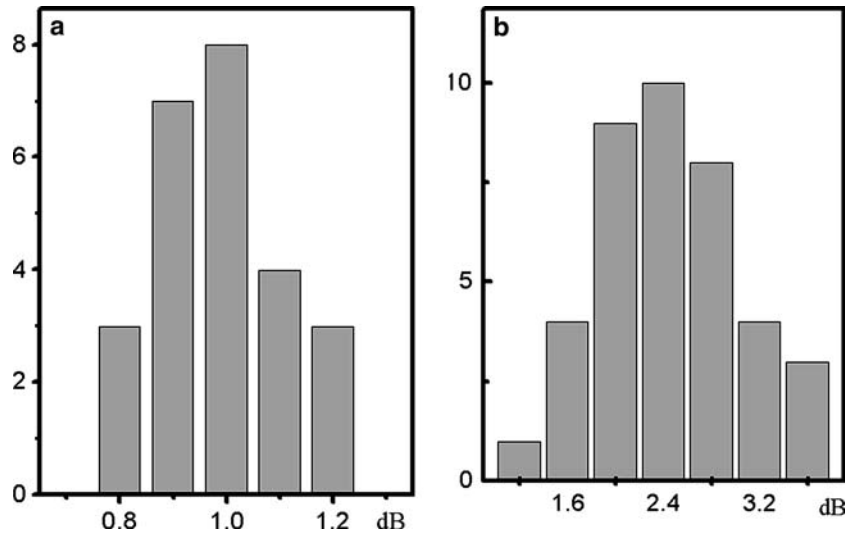
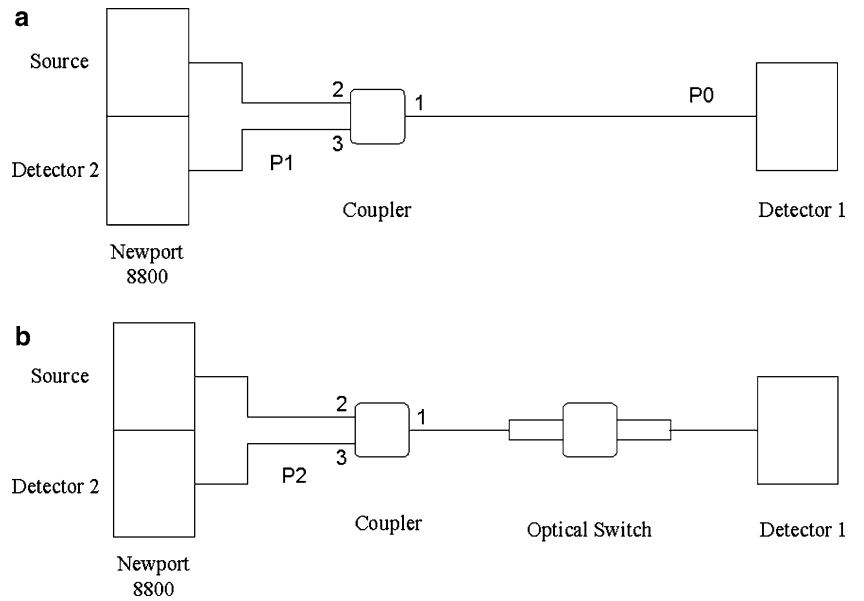


Fig. 9 Measurement set-up of return loss



were measured in Fig. 9a. In order to reduce the reflection from detector 1, the fiber between port 1 and detector 1 was wrapped in mandrel with a diameter of 15 mm when the readings of P_1 were taken. Subsequently the detector was disconnected from coupler P_1 . Then the switch was connected to coupler port 1, and the detector as shown in Fig. 9b. The mandrel wrap of 15 mm of the optical fiber between the switch and detector 1 was applied to reduce the reflection when the readings of P_2 were taken. The calculation of return loss is formulated (TIA/EIA standard 1999) as

$$RL = -10\text{Log}_{10}\left[\frac{P_2 - P_1}{P_0}\right] - IL, \quad (4)$$

where, RL is the return loss; IL is the coupler insertion loss; P_0 , P_1 and P_3 are the readings of power described above. Following above method, the return loss of optical switch was characterized. The readings were

taken repeatedly to minimize the errors caused by the connect difference. The characterization results and their distribution are depicted in Fig. 10. The results include bar state and cross state.

The crosstalk is the fraction of power transferred from input port i to an unintended output port j expressed in the unit of dB. Crosstalk depends on the input and out put ports (i, j), wavelength, and may also depend on the switch state. The crosstalk, $XT_{ij}(\lambda)$, from input port i to output port j at wavelength λ and for a given switch state is defined by the following equation (generic requirements for singlemode fibre optic switches 2001):

$$XT_{ij}(\lambda) = -10\text{Log}_{10}\frac{P_j(\lambda)}{P_i(\lambda)}, \quad (5)$$

where, $P_i(\lambda)$ is the optical power launched into port i at center wavelength λ and $P_j(\lambda)$ is the off-state (i.e., when

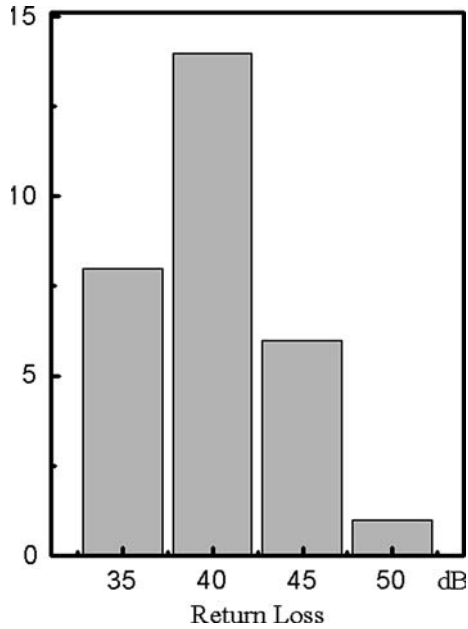


Fig. 10 Return losses and their distribution

connection (i, j) is in the off-state) optical power measured at port j at center wavelength λ and a given switch state. The results of the crosstalk test for the optical switch were over 35 dB in the cross state and over 60 dB in the bar state.

A switching time testing system was constructed through the integration of instruments based on the

Labview 6.1 platform. Figure 11 shows the instrument connection diagram of the system. From the main panel, the user can control the configurations of instruments, including laser sources, power meter, function generator and oscilloscope.

Keithley 2400 was used to generate the continuous pulse wave as the control signal to the optical switch. After receiving the control signal, a mirror in the MEMS optical switch moved into the optical path, which took time t_1 for port B to receive output light. When the Newport PTS-FOPM dual-channel power meter received the output signal from the optical switch, it took time t_2 to send the power value to A/O port, which had the magnitude of ns and was limited by the instrument performance.

The control signal can be continuously read from CH1, while Tektronix TDS-210 can receive the signal from the A/O port of PTS-FOPM from CH2. The time difference between the control signal and the signal from A/O port of PTS-FOPM dual power meter is $T = t_1 + t_2$, which was considered as switching time.

Thus the electrical control signal of the optical switch and the optical response can be acquired and analyzed, as illustrated in Fig. 12, where the switching time was read as around 5.5 ms.

4 Conclusion

In summary, a packaging solution for fiber optic MEMS devices was demonstrated, which is applicable for those devices embedded with fiber grooves. The implement of

Fig. 11 Instrument connection diagram

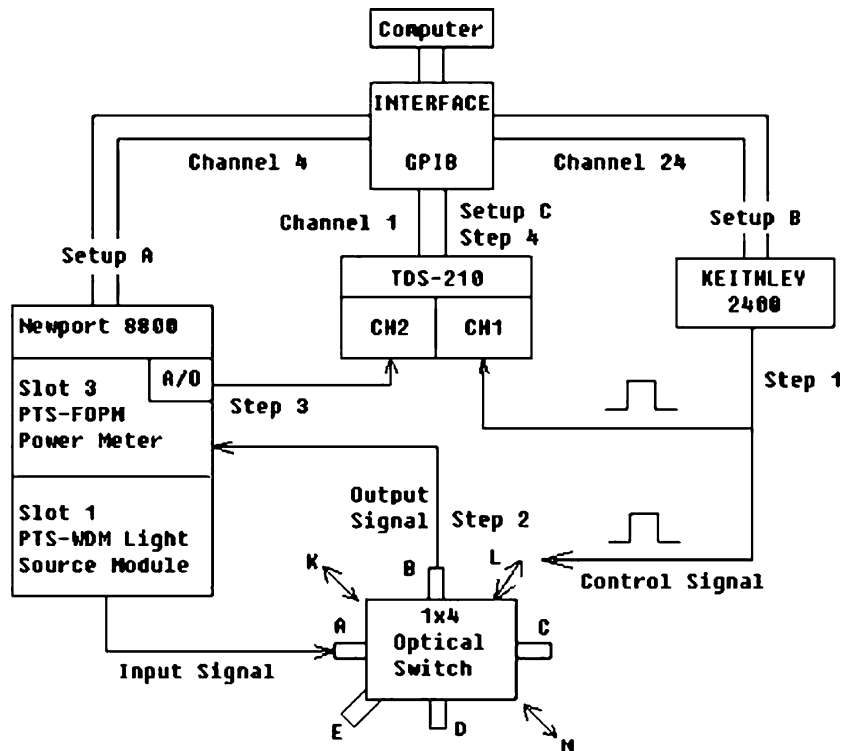
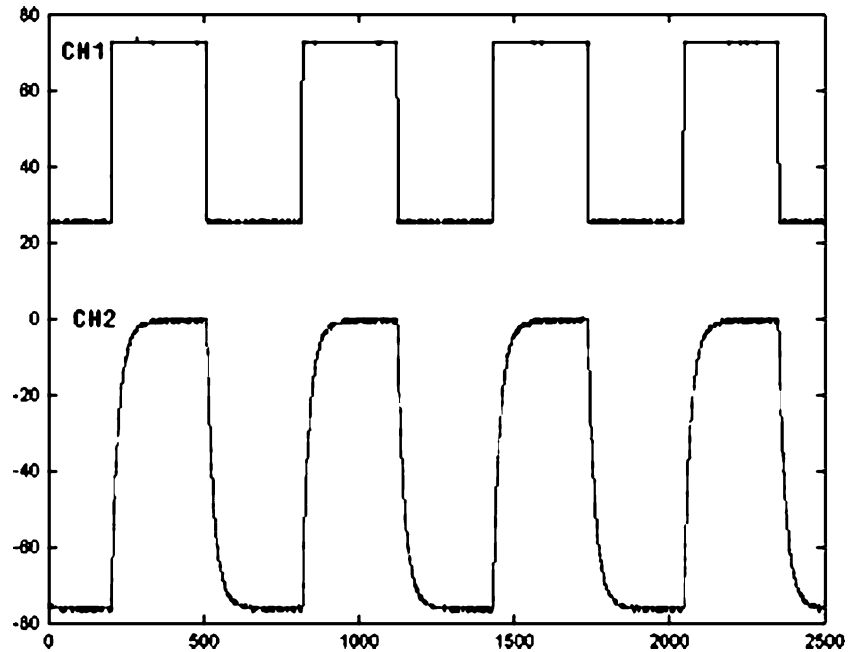


Fig. 12 Control versus optical signals: optical switch



the two-level packaging scheme enhanced the protection towards the delicate optical MEMS device. Passive fiber alignment with an accuracy comparable with active alignment was presented by the combination of rectangular shape fiber grooves and micro fiber stoppers. Experimental setups for fiber assembly, fiber coupling test and switching test were successfully conducted as well.

Acknowledgement The authors would like to thank the staff at Sensors, actuators, and Microsystems Laboratory (SAMPLAB), Institute of Microtechnology, University of Neuchâtel, Switzerland, for their technical support and the microfabrication of optical MEMS devices. The project was funded by the Agency for Science, Technology and Research (A*STAR), Singapore.

References

- Generic requirements for singlemode fiber optic switches (2001) Telcordia Technologies GR-1073-core
- Jin YF, Wang ZF, Wang ZP (2002) A study on hermetic packaging for micro-optical switch. Proceedings of IEEE 4th electronics packaging technology conference, Singapore, 2002, pp 96–100
- TIA/EIA standard (1995) Interconnection device insertion loss test, TIA/EIA-455-34A
- TIA/EIA standard (1999) Determination of component reflectance or link/system return loss using a loss test set, TIA/EIA-455-107A
- Wang ZF, Shan XC, Wang ZP, et al (2002) Development of a new 1×4 optical switch. In: Proceedings of DTIP, Cannes, SPIE Vol. 4755, pp 544–548